Thermal, Electron, and Photon Induced Chemistry of Acetone on Ag(111)

Stacy Converse Sparks, Andras Szabo, G. J. Szulczewski, K. Junker, and J. M. White*

Department of Chemistry and Biochemistry, Center For Materials Chemistry, University of Texas, Austin, Texas 78712

Received: June 19, 1997; In Final Form: August 11, 1997[⊗]

Acetone, $(CH_3)_2CO$ and $(CD_3)_2CO$, adsorbed on Ag(111) at 95 K was studied using using thermal, photon, and electron activation. Adsorption and desorption involve no dissociation. The temperature-programmed desorption (TPD) spectra exhibit three resolvable peaks, two of which (146 and 134 K) are assigned to the first layer and the third (127−134 K) to multilayers. TPD, after sequentially dosing 1 ML of $(CD_3)_2CO$ followed by 1 ML of $(CH_3)_2CO$, shows extensive mixing of the two adsorbates throughout the full width of the desorption peaks. This suggests rapid motion, on the TPD time scale, below the onset of desorption (120 K). RAIRS analysis at 95 K indicates that the orientation of adsorbed acetone is coverage-dependent, but the C═O bond remains nearly parallel to the Ag(111) surface at all coverages. At the lowest coverages the average C−C−C plane position is 50° from the surface normal; at higher coverages (up to monolayer) this plane tilts toward the surface normal (22°). Dissociation and desorption of adsorbed $(CH_3)_2CO$ are initiated by 100 eV electrons; TPD products include ketene, methane, and high-temperature $(CH_3)_2CO$ derived from acetone enolate. RAIRS after electron irradiation provides evidence for electron-induced reorientation in which the C═O bond moves away from the surface plane. The cross section for loss of parent was of order 10^{-16} cm^2. Photon irradiation at 248 and 193 nm produced no effects with cross sections higher than 10^{-21} cm^2.

I. Introduction

Acetone, CH_3COCH_3, is the simplest ketone and is widely used as a solvent. It is liquid at room temperature and does not readily form molecular crystals; to our knowledge, the crystal structure of acetone has not been reported. The adsorption of CH_3COCH_3 has been examined on several well-characterized metal and nonmetal substrates including Pt,[1] Al_2O_3,[2] Ag,[3] Cu,[4] Ru,[5] NaCl,[6] and Si.[7] Thermal activation is substrate-dependent. On the coinage metals, there is no evidence for surface decomposition unless atomic oxygen is present. On surface reconstructed Si(100), there is good evidence for di-σ-bonding across the substrate's dimer rows. On Ru(0001), a relatively aggressive metal, thermal decomposition leads to surface C and O. On Pt(111) there is little dissociation, but there is evidence for a resolvable bilayer that desorbs at a temperature between those of the multilayer and monolayer.

Since Ag(111) interacts weakly with many molecular adsorbates, we anticipated, and found, that CH_3COCH_3 absorbs and desorbs without dissociation. As we demonstrate here using temperature-programmed desorption (TPD) spectroscopy, the attractive interaction between CH_3COCH_3 molecules does not differ significantly from the interaction between CH_3COCH_3 and Ag(111). In such situations, there are several adsorbate structures with nearly the same stability, and the orientation of adsorbates adjacent to the substrate is often a strong function of the local coverage. For example, several recent studies on the orientation of weakly physisorbed hydrocarbons and alkyl halides on metal and ionic salt surfaces show the following trend: at coverages significantly lower than one monolayer (ML), the molecules adsorb with the major axis of the molecule parallel to the surface, while at, or near, monolayer coverage the major molecular axis tilts away from the surface.[8−13]

Photon- and electron-induced surface chemistries of adsorbates are of considerable interest and are explored here as part of an ongoing program in our laboratory. In the absence of thermal activation, such nonthermal processes are easily identified.

In the present work the adsorption and orientation of acetone, CH_3COCH_3, and perdeuterated acetone, CD_3COCD_3, on Ag(111) are examined. There is no evidence for thermally activated bond breaking in the adsorbate. Based on reflection−absorption IR spectroscopy (RAIRS), acetone follows the trend of other molecules; at low coverages the C−C−C plane lies 50° away from the surface normal, while at monolayer coverage it lies only 22° away from normal. At all coverages, the average orientation of the carbonyl (C═O) group is parallel to the surface. Electron irradiation (100 eV) leads to bond dissociation, desorption, and reorientation of the remaining carbonyl groups with a cross section of order 10^{-16} cm^2. Even though molecular acetone adsorbs, there is no evidence for photon-driven bond breaking of adsorbed CH_3COCH_3 at 248 and 193 nm.

II. Experimental Section

Most of these experiments were performed in a two-level ultrahigh-vacuum (UHV) system. The upper level is equipped with an Mattson Cygnus 100 Fourier transform infrared (FTIR) spectrometer, an Ar^+ sputter gun used to clean the sample, and, for electron irradiation, a filament source (see below). The lower chamber has a Physical Electronics single-pass CMA Auger electron spectrometer (AES) and a differentially pumped (5 mm aperture) Extrel C-50 quadrupole mass spectrometer (QMS). The geometry of this two-level system and the differentially pumped quadrupole preclude line-of-sight detection of electron stimulated desorption.[14] The base pressure is (3−4) × 10^{-10} Torr. The main chamber is pumped with a 330 L/s turbopump, the quadrupole with a 130 L/s turbopump, and the dosing line with a separate 130 L/s turbopump.

The silver crystal was oriented and cut, within 1° of the (111) plane, and then polished with 1.0 μm diamond paste. The crystal was clipped to the mount by the spring force of a

[⊗] Abstract published in *Advance ACS Abstracts,* September 15, 1997.

S1089-5647(97)02005-1 CCC: $14.00

U-shaped piece of 0.75 mm diameter W wire. To measure the sample temperature, a chromel−alumel thermocouple was attached to the substrate. Direct spot-welding to Ag(111) is difficult, so the thermocouple was first sandwiched into a folded piece of 0.05 mm thick Ta foil. After spot-welding across the Ta, this foil was sandwiched into a bent silver wire that was spot-welded to the back of the sample. The sample temperature was varied between 83 and 700 K. A helium bubbling technique[15] lowered the temperature 5 K from the lowest temperature (88 K) obtained with liquid N_2 alone.

The sample was cleaned by Ar^+ bombardment (4 kV, 10 mA, 5 min) followed by annealing to 700 K for 5 min. After this treatment, no contaminants appeared in AES.

The acetone (EM Science, 99.5% pure) was dried over calcium carbonate. The acetone-d_6 (Isotec Inc., 99.9% D) was used as received. The samples were subjected to freeze−pump−thaw cycles to remove dissolved air, and residual gas analysis confirmed the purity of the dosed material. Both adsorbates were dosed through a 3 mm i.d. stainless steel tube that terminates ∼2.5 cm in front of the surface. Exposures were based on the time in front of the doser after establishing a reproducible pressure rise measured by an ion guage. All exposures are reported in the units of "effective" Torr s, calculated by multiplying the ion gauge reading by the duration of exposure. Since the pressure gauge sensitivity to acetone and the proximity focusing of the doser tube are not known, we report no absolute exposures (langmuirs).

TPD spectra were taken in line-of-sight configuration and relative coverages determined by integrating the area under desorption peaks. Ramp rates between 0.5 and 3 K s^{-1} were used, with lower ramp rates providing more accurate desorption temperatures and better peak resolution. The temperature ramp was computer-controlled, and the mass spectrometer was multiplexed. The fragmention pattern of acetone determined for our system agreed with published patterns.[16] To track parent desorption, the most intense ion, 43 amu, was measured.

The RAIRS data were taken with a resolution of 4 cm^{-1} over a range of 800−4000 cm^{-1}. For each spectrum, 2000 scans were averaged, corresponding to a data acquisition time of 8 min. An absorbance noise level $\sim 5 \times 10^{-5}$ was routinely achieved. RAIRS peaks were least-squares fit using a combination of Gaussian and Lorenzian peaks. For comparison, a gas-phase IR spectrum was taken. In this case, acetone was introduced into the nitrogen-purged FTIR spectrometer rather than into the UHV system itself; as shown below, this spectrum contains a small amount of water.

A heated tungsten filament placed 5 cm from the sample in the upper chamber served as the electron irradiation source. The incident energy was 100 eV, set by a bias applied between the filament and the sample. The current from the sample to ground was typically 15 μA. Since this measurement does not account for scattered primary and secondary electrons, the currents are lower limits and the reported cross sections are upper limits. Some radiation from the filament was incident on the substrate but raised the base temperature no more than 2 K, insufficient to desorb CH_3COCH_3.

As will become clear, electron irradiation led to loss of parent and to interesting but very broad TPD spectra, which limited detailed product analysis. To gain further insight, we used a separate instrument equipped with Mg Kα X-rays and a double-pass CMA to gather a few XP spectra before and after electron irradiation and with heating. The dosing temperature was 100 K.

We also examined briefly the photochemistry initiated by 193 and 248 nm excimer laser pulses in adsorbed acetone. These experiments employed an instrument capable of measuring TPD spectra and time-of-flight distributions of species ejected by these laser pulses.[17]

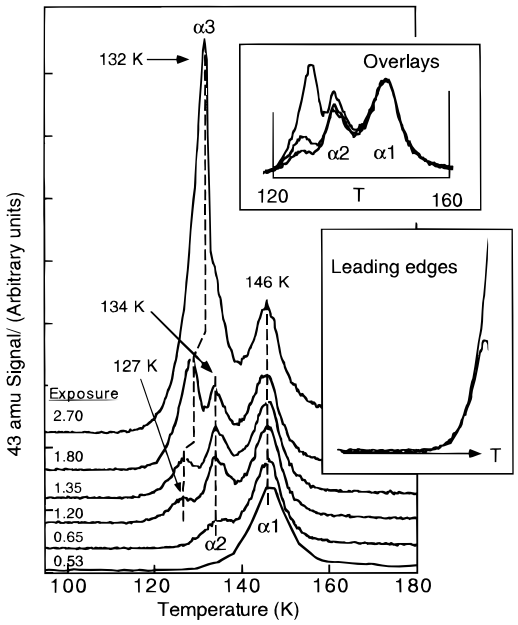

Figure 1. Dosed at 90 K, thermal desorption spectra of $(CH_3)_2CO$ from Ag(111); exposure of the samples is indicated in 10^{-6} Torr s. The heating rate was 0.5 K/s. The upper inset shows the overlap of the TPD for the curves between 1.20×10^{-6} and 1.80×10^{-6} Torr s. The lower inset show the leading edge overlap of the 1.8×10^{-6} and 2.7×10^{-6} Torr s experiments.

III. Results

Temperature-Programmed Desorption. TPD traces, following the 43 amu CH_3CO^+ signal, are shown in Figure 1 for several coverages of acetone; effective exposures are indicated on each curve. The only other ion signals tracked the 43 amu intensity with the pattern of CH_3COCH_3, and after TPD, AES showed a surface free of C and O. At the lowest exposure, 0.53 Torr s, there is one symmetric peak at 146 K (α1). With increasing exposure, a second peak grows in at 134 K (α2), and at even higher exposures a third peak is observed at 127 K (α3). Both the α1 and α2 TPD peaks are saturated for 1.20, 1.35, and 1.80 Torr s exposures (upper inset). As described below, we define monolayer coverage in terms of saturation of both α1 and α2. The same three peaks were observed for acetone-d_6 (not shown), and the peak temperatures were identical to within ±2 K.

The α3 peak does not saturate, and its position moves to higher temperatures with increasing exposure, indicating desorption from multilayers. As expected for zero-order multilayer desorption, the 2.70 Torr s curve is asymmetric, decaying more sharply than it rises (dashed vertical line at 132 K). Further, the leading edges of the 1.80 and 2.70 Torr s curves align (lower inset). The multilayer peak temperature compares nicely with literature values, taking into account differences in heating rates. Acetone multilayers are reported to desorb at ∼137 K from both Pt(111) (β = 1 K/s) and Ag(110) (β = 6 K/s).[1,3] Other experiments on Pt(111) reported multilayer desorption at 149 K (β = 3 K/s) and on Si(100) at 130 K (β = 4 K/s).[1,7]

Figure 2 uses an extensive data set, including data from Figure 1, to show the mass 43 total peak intensity and the intensity of each individual peak (α1, α2, and α3) plotted as a function of total surface exposure. Note that the *Y*-axis scaling differs to enhance the features. The α1 peak intensity rises sharply and

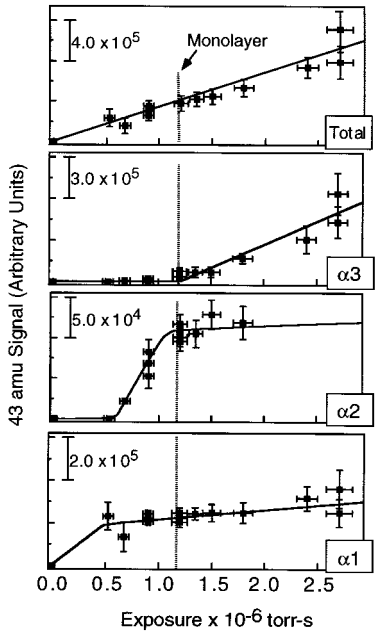

Figure 2. Integrated TPD area versus total exposure for the α1, α2, and α3 peaks and the total area for all peaks. Dosing temperature = 90 K.

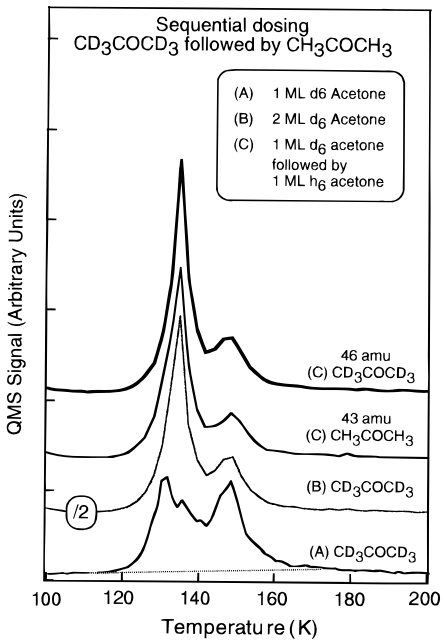

Figure 3. TPD spectra for three experiments: (A) 1 ML of CD_3COCD_3, (B) 2 ML of CD_3COCD_3, and (C) 1 ML of CD_3COCD_3 followed by 1 ML of CH_3COCH_3. The dosing temperature was 90 K.

approaches saturation at approximately 0.5×10^{-6} Torr s, where the α2 peak intensity begins to rise. Significantly, α2 growth slows when its intensity reaches about half that of the α1 peak. Before the α2 peak saturates, the multilayer slowly begins to grow, making it experimentally impossible to prepare an adsorbate coverage that saturates α2 with no contribution from α3. The latter intensity grows more rapidly after α2 saturates.

Within measurement uncertainty, the total intensity, top panel, is linear with exposure (and passes through the origin); i.e., the sticking coefficient does not change markedly in passing from submonolayer to multilayer coverage. Thus, exposure can be easily correlated with coverage. According to our model (see Discussion), the maximum monolayer coverage is reached when α2 saturates and corresponds to an exposure of 1.2×10^{-6} Torr s (dashed line in Figure 2); we designate this exposure as 1 ML and, from this point on, report coverages in ML units. As indicated in Figure 1, a small amount of multilayer desorption appears in TPD following this exposure.

Some insight into the nature of acetone monolayers and multilayers can be gained by sequential dosing of isotopically labeled species, i.e., $(CD_3)_2CO$ followed by $(CH_3)_2CO$. Figure 3 summarizes the TPD data for three experiments dosed at 90 K: (A) 1.0 ML of $(CD_3)_2CO$, (B) 2 ML of $(CD_3)_2CO$, and (C) 1.0 ML of $(CD_3)_2CO$ followed by 1 ML of $(CH_3)_2CO$. The curve for case B is scaled by a factor of 2. The α2 peak is overwhelmed by the multilayer after a 2 ML dose (curve B). The key observation is extensive mixing in curves C, evident throughout the whole TPD spectrum. There is no evidence for preserving the dosing order; from the leading edge to the trailing edge, each isotopic component makes a nearly equal contribution. We conclude that, on the time scale of dosing *and heating from 90 to 115 K* (order of magnitude 10^2 s), there is extensive mixing among the molecules occupying the monolayer and multilayer states.

RAIRS of CH_3COCH_3 and CD_3COCD_3. The gas-phase infrared absorption spectra (curve a) and the RAIRS (curve b) for 4.5 ML of acetone dosed on the Ag(111) surface are shown in Figure 4. The background ($\sim 1 \times 10^{-2}$) in the gas-phase spectrum between 1400 and 1700 cm^{-1} is from water and is due to the backfilling method (see Experimental Section) by

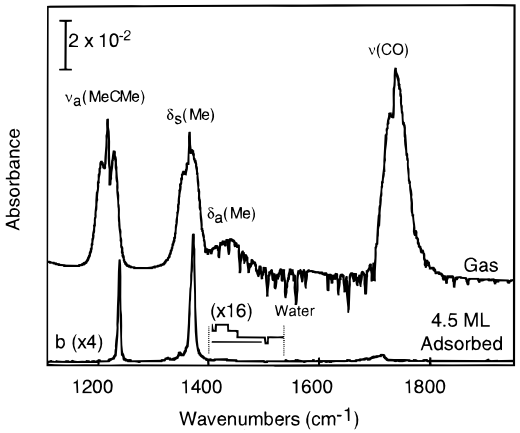

Figure 4. RAIRS of gas phase (a) and 4.5 ML of adsorbed (b) CH_3COCH_3 on Ag(111).

which acetone was introduced into the spectrometer. There are four acetone bands—1180−1280, 1330−1400, 1400−1470, and 1690−1810 cm^{-1}—whose breadths reflect rotational states. The dominant mode of motion for each band is antisymmetric $H_3C-C-CH_3$ stretch (ν_a(MeCMe)), symmetric methyl in-plane bending (δ_s(Me)), antisymmetric methyl in-plane bending (δ_a(Me)), and the carbonyl stretch (ν(CO)).[13] In addition to these vibrational modes, the gas-phase spectra showed absorption, weaker than δ_a(Me), in the C−H stretch region of 2900−3040 cm^{-1}.

The multilayer RAIRS (note the 4× scale factor of curve b) exhibits only three bands. The positions compare favorably with the gas-phase spectra and are much narrower since rotational motion is hindered. We assign absorption in the 1660−1730 cm^{-1} range to ν(CO), the 1220−1250 cm^{-1} range to ν_a(MeCMe), and the 1355−1400 cm^{-1} range to δ_s(Me).[1,3,18] Not surprisingly, upon scale expansion (×16), the δ_a(Me) vibrational mode is observable but very weak. It is immediately apparent, and central to the discussion below, that ν(CO) is relatively weak in curve b. This indicates, as discussed below, the preferred adsorbate orientation in multilayers: CH_3COCH_3 adsorbs with the carbonyl bond nearly parallel to the Ag(111) surface.

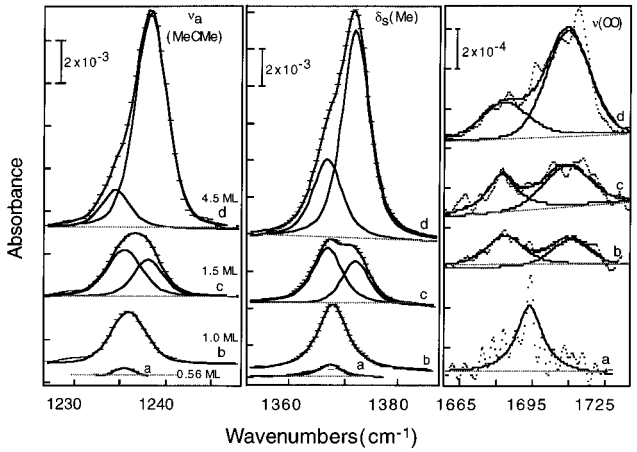

Figure 5. High-resolution RAIRS of (a) 0.56, (b) 1.0, (c) 1.5, and (d) 4.5 ML of CH_3COCH_3 adsorbed on Ag(111) at 95 K. Note the differing scale factors for the three panels.

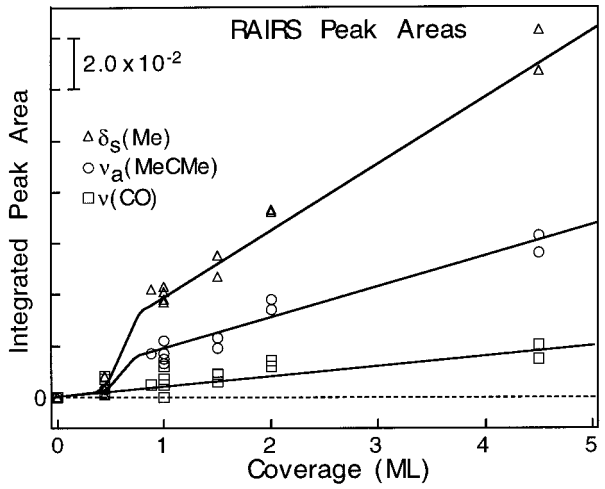

Figure 6. RAIRS peak areas as a function of coverage for the three strongest vibrational modes of adsorbed CH_3COCH_3 on Ag(111) at 95 K.

Figure 5 shows more detailed RAIRS for four coverages from 0.56 to 4.5 ML. With one exception, the experimental curves have been empirically fit to the minimum number of components (one or two) required to span the absorbance region and exhibit the indicated structure. Curve c in the left-hand panel is the exception; for reasons outlined below, two curves were used even though a single broad peak would suffice. At the lowest coverage, 0.56 ML, the three regions, while weak, are each readily fit with a single peak.[19] Doubling the coverage (1.0 ML) splits only the ν(CO) region, while tripling the coverage, 1.5 ML, splits δ_s(Me) and ν(CO) and broadens ν_a(MeCMe) such that two bands are reasonable. The splitting of ν_a(MeCMe) is more obvious at 4.5 ML, where a shoulder is evident on the low-frequency side. Qualitatively, except for the lowest coverage a, the ν(CO) absorbance is 10 times weaker than the others.

Using data like those of Figure 5, integrated peak areas were calculated and plotted versus coverage (Figure 6). In the high coverage regime, between 1 and 4.5 ML, the three absorbances grow linearly, and the peak areas are ordered δ_s(Me) > ν_a(MeCMe) > ν(CO). For monolayer coverage, the absorbance intensity ratio follows the pattern δ_s(Me):ν_a(MeCMe):ν(CO) :: 1:0.5:0.14. As the coverage decreases from 1 to 0.56 ML, the relative intensities change dramatically, becoming more nearly equal (Figure 5a). For all coverages, the slope of the ν(CO) line is a constant $(4 \pm 1) \times 10^{-3}$ absorbance units/ML, while the ν_a(MeCMe) and δ_s(Me) slopes start out as comparable, show

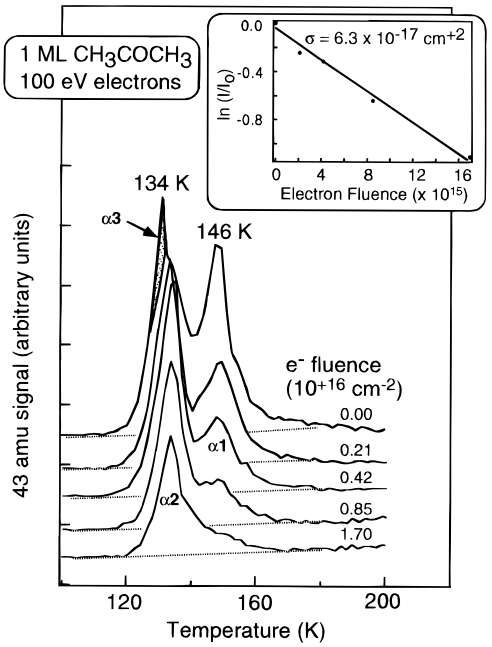

Figure 7. Effect of 100 eV electrons on TPD of 1 ML of CH_3COCH_3 on Ag(111). Inset shows, in semilog form, the decay of the acetone TPD peak area (total) as a function of fluence.

a steep increase in intensity between 0.5 and 1.0 ML, and then level out to slopes of $(1.3 \pm 0.3) \times 10^{-2}$ and $(2.5 \pm 0.5) \times 10^{-2}$ absorbance units/ML, respectively. The sharp increase corresponds, in TPD, to saturation of α1 and growth of α2.

As noted above, the RAIRS bands split at coverages $\geq$1 ML. For ν(CO), two peaks of approximately equal area appear at 1 ML (Figure 5). With increased coverage, the higher frequency component grows while the lower frequency component remains nearly constant. For the other two modes, the splitting is not apparent at 1 ML but is obvious in δ_s(Me) at 1.5 ML, where two peaks of nearly equal intensity give a satisfactory fit. At this exposure, the ν_a(MeCMe) can also be fit nicely with two peaks of equal intensity. For 4.5 ML, absorbance increases preferentially in the high-frequency component of each of the three modes. The δ_a(Me) mode was very weak at all coverages but showed the same qualitative behavior as ν(CO), i.e., slow increase with coverage and no sharp change in the 0.5−1 ML region.

Electron Irradiation. Figure 7 shows the 43 amu TPD signal taken after irradiation of 1 ML of CH_3COCH_3 with different fluences of 100 eV electrons, as indicated on each curve. In each experiment, the α1 and α2 states were initially fully saturated, and there was always a small, but unavoidable, α3 (multilayer) state population (dotted region of Figure 7). With increasing fluence, the total peak area decays, the α1 more rapidly than the α2 region. The average cross section describing the decay of the total TPD area is $(6.3 \pm 0.2) \times 10^{-17}$ cm^2 (straight line, inset of Figure 7). This cross section depends weakly on coverage; for multilayer coverages, it is slightly higher, $(6.7 \pm 0.2) \times 10^{-17}$ cm^2, and for submonolayer coverages, slightly lower, $(5.8 \pm 0.2) \times 10^{-17}$ cm^2.

Figure 8 shows, for several masses, postirradiation TPD spectra taken after three different initial coverages were each irradiated with 3.53×10^{16} e$^-$ cm^{-2}. Note that the ordinate scales in panels B (0.75 ML) and C (0.56 ML) are decreased by a factor of 2. For panel A (2.25 ML), all signal ratios in the 137 K peak are consistent with CH_3COCH_3 desorption attributable to a residual multilayer. The α1 state at 146 K does not appear, and a new and very broad peak sets in around 150 K and extends to 350 K, with a peak at 190 K. While primarily

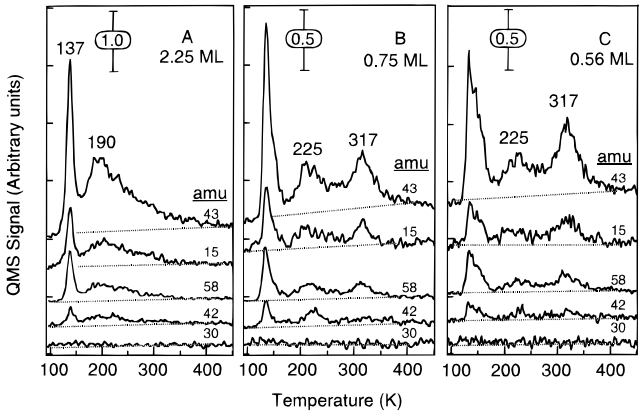

Figure 8. TPD taken after 100 eV electron irradiation of (A) 2.25, (B) 0.75, and (C) 0.56 ML of adsorbed CH_3COCH_3. Note the scale differences in the three panels.

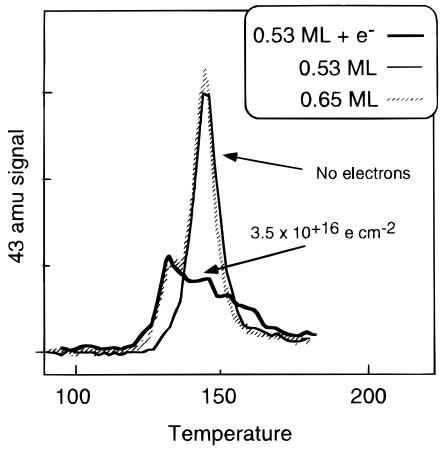

Figure 9. Three TPD spectra, one involving electron irradiation.

attributable to CH_3COCH_3 desorption, the intensity ratios of the 15 and 42 amu signals change with respect to the 43 amu signal between 150 and 300 K (not shown). The 15 amu relative intensity is higher below 190 K while the 42 amu relative intensity is higher above 190 K. The excess 42 amu signal is consistent with ketene ($H_2C{=}C{=}O$) desorption (mixed with acetone). The excess 15 amu signal is attributed to CH_4 desorption that peaks between 185 and 195 K. These assignments are consistent with results using other adsorbates, e.g., biacetyl,[14] methyl formate,[20] and methanol[21] where this temperature region is better resolved.

An important change occurs as the initial coverage drops; the 190 K peak is replaced by two local maxima at 225 and 317 K (panels B and C of Figure 8). The 317 K peak increases as the initial coverage decreases from 0.75 to 0.56 ML. After removing small 42 and 15 amu contributions due to ketene and methane, both these high-temperature peaks are attributable, on the basis of mass fragmentation patterns, to *reaction-limited acetone formation* followed by prompt desorption. We propose an enolate as the surface precursor. Finally, although we did not measure the H_2 desorption profiles, a later experiment (not shown) using (CD_3 $COCD_3$) did detect D_2 evolution between 200 and 240 K.

To this point the following picture emerges. Electron irradiation of adsorbed CH_3COCH_3 leads to dissociation with some retention of fragments. Upon heating, there is desorption of ketene, methane, and acetone, all formed by reactions among dissociated fragments. Figure 9 demonstrates that accumulation of fragments shifts some parent intensity into less tightly held states. Two TPD spectra without irradiation are shown; the 0.65 ML case has an α2 shoulder on the low-temperature side, while the 0.53 ML case does not. After irradiation, the 0.53 ML TPD contains the α2 shoulder indicative of a shift from α1 to α2 induced by the electron exposure. For the 0.75 and 2.25 ML cases of Figure 8, we see a similar shift with fragment accumulation, in these cases into α2 or α3.

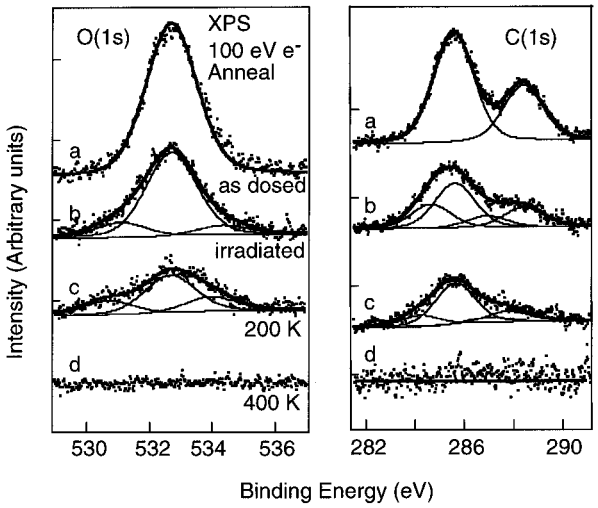

Figure 10. Core level XPS data for monolayer CH_3COCH_3 before (a) and after (b) irradiation with 0.85×10^{16} e^- cm^{-2}. Subsequently, the irradiated sample was heated to 200 (c) and 400 K (d).

XPS measurements offer further insight. The O(1s) and C(1s) XPS spectra for 1 ML of acetone, before and after electron irradiation and after annealing to 200 and 400 K, are shown in Figure 10 and summarized in Table 1. Before irradiation (curves a), both C(1s) and O(1s) have the expected characteristics for molecularly adsorbed CH_3COCH_3; O(1s) has a single symmetric peak at 532.7 eV, and C(1s) peaks at 285.6 (methyl) and 288.4 eV (carbonyl) with a 2-to-1 intensity ratio.

After irradiation with 0.85×10^{16} e^- cm^{-2}, curves b, both signals become weaker, indicating loss of C and O during irradiation, and broader, indicating new chemical environments. The C(1s) signal drops to 65% and the O(1s) to 73% of their initial values. We propose, on the basis of results with $CH_3COCOCH_3$,[14] that both CO and CH_3 are ejected. The peak positions, after irradiation, are consistent with formation of products with lower C(1s) BE and both lower and higher O(1s) BE. Three states for O(1s)—531.1, 532.7, and 534.4 eV—and four for C(1s)—284.6, 285.6, 286.9, and 288.4 eV—are identified. The higher BE O(1s) is assigned to a di-σ-bonded form of acetyl, $C_{(a)}O_{(a)}CH_3$,[22] and the low BE O(1s) to the enol form of the parent, $CH_3CO_{(a)}H(CH_2)$. The low BE C(1s) signal is assigned to a C═C moiety, consistent with the proposed enol.

Annealing to 200 K, curves c, reduces O(1s) by an additional 21% and C(1s) by 19%, i.e., nearly equal fractions, consistent with removal of parent. Most of the O(1s) loss occurs in the central O(1s) peak assigned to acetone. Similarly, there is significant C(1s) loss in the high BE region corresponding to carbonyl removal. In the methyl C(1s) region, losses are smaller, suggesting significant contributions from species other than parent, e.g., $C_{(a)}O_{(a)}CH_3$ or $C_{(a)}H_3$.

Annealing to 400 K, curves d, removes all the detectable C(1s) and O(1s). In the C(1s) spectrum, the signal does appear to rise slightly above the baseline around 286 eV (there are relatively few points below the flat baseline), from which we conclude that at 400 K no more than 2% of the original amount of C remains.

RAIRS after Electron Irradiation. Figure 11 shows RAIRS of 0.75 ML of CH_3OCH_3 taken at 90 K before and after electron

TABLE 1: XPS Core Level Binding Energies and Intensities of Acetone on Ag(111) Irradiated with 100 eV Electrons

	C(1s) peak positions and relative intensities						O(1s) peak positions and relative intensities			
expt	C(1s) total area	284.2−284.6	285.6	286.9−287.1	287.8	288.4	O(1s) total area	530.7−531.1	532.7	534.0−534.4
dose at 120 K	1.00	0	0.65	0	0	0.35	1.0	0	1	0
irradiated at 120 K	0.65	0.13	0.26	0.07	0	0.12	0.73	0.10	0.55	0.08
irradiated at 200 K	0.46	0.08	0.26	0.04	0.08	0.0	0.52	0.10	0.28	0.14
irradiated at 400 K	0.00	0	0	0	0	0.0	0.00	0	0	0

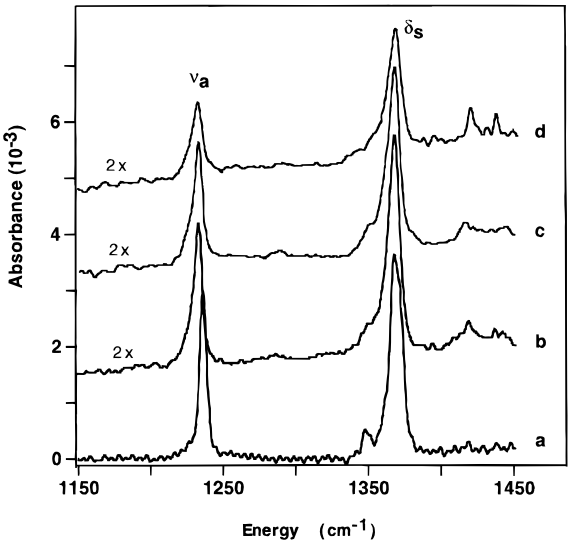

Figure 11. RAIRS before (a) and after 100 eV electron irradiation of 0.75 ML of CH_3COCH_3 with (b) 2.8×10^{15}, (c) 5.6×10^{15}, and (d) 11.2×10^{15} e^- cm^{-2}.

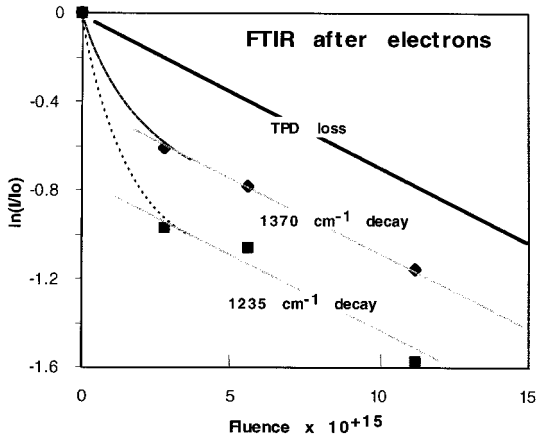

Figure 12. On a semilog plot, the peak areas for the 1370 and 1235 cm^{-1} vibrational bands as a function of electron fluence beginning with 0.75 ML of adsorbed CH_3COCH_3. For comparison, the TPD decay is also shown.

irradiation for 30−120 s ($(2.8-11.2) \times 10^{+15}$ e^- cm^{-2}). Several observations emerge from these spectra. With increasing electron irradiation, (1) the intensities of the modes decrease monotonically, (2) the asymmetric Me−C−Me stretching mode shifts to lower frequency (1236.4−1234.0 cm^{-1}) and broadens (5.4−8.7 cm^{-1}), (3) the small peak on the low-frequency side of the symmetric CH_3 deformation mode either vanishes or shifts to higher frequency and becomes buried in the more intense δ_s CH_3 mode, and (4) the symmetric CH_3 deformation mode does not shift (1368.1 cm^{-1}) or broaden (9.8 cm^{-1}). There are two small peaks between 1400 and 1450 cm^{-1} which we have been unable to assign.

Figure 12 shows, in semilog form, how the intensities of the two strong infrared bands, $\delta_s(CH_3)$ and ν_a(MeCMe), vary with electron fluence. Also shown is the same plot for the loss of parent TPD signal. The linear portions of the lower two curves are parallel to the curve describing the TPD loss. TPD and RAIRS track each other faithfully over much of the irradiation. But clearly, in the early stages, vibrational bands decay much more steeply than does the TPD. We take this as evidence for electron-induced restructuring of some of the adsorbed CH_3COCH_3, a process competing with dissociation and desorption. This is not a simple coverage effect because $\delta_s(CH_3)$ at 1370 cm^{-1} decays less than the ν_a(MeCMe) at 1235 cm^{-1}; were the effect due to coverage, the largest change would occur in $\delta_s(CH_3)$ according to Figure 6.

Comparing the C−O stretch, ν_{CO}, before and after electron irradiation of 0.75 ML of CH_3COCH_3 (Figure 13) provides further evidence for electron-induced restructuring. The striking result of electron irradiation, curves b and c, is the intensification of the carbonyl region even though the total coverage of CH_3COCH_3 is dropping. We take this as substantiating an electron-initiated reorientation of the carbonyl group of adsorbed acetone.

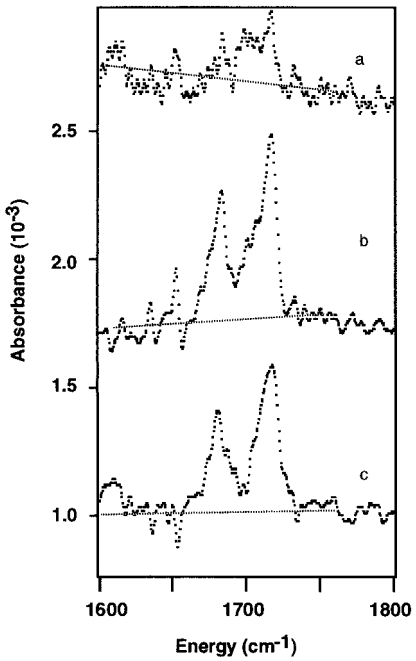

Figure 13. Carbonyl stretching region before (a) and after electron irradiation of 0.75 ML of CH_3COCH_3 with (b) 2.8×10^{15} and (c) 5.6×10^{15} e^- cm^{-2}.

Photon Irradiation. To compare nonthermal activation with incident photons and electrons, we prepared various coverages 1−20 ML of CH_3OH and irradiated them with 193 nm (6.4 eV) or 248 nm (5.0 eV) excimer laser pulses at 100 K. For these experiments, the sample was irradiated at 20 Hz for 5000−20 000 shots at a maximum of 8 mJ cm^{-2}. The calculated

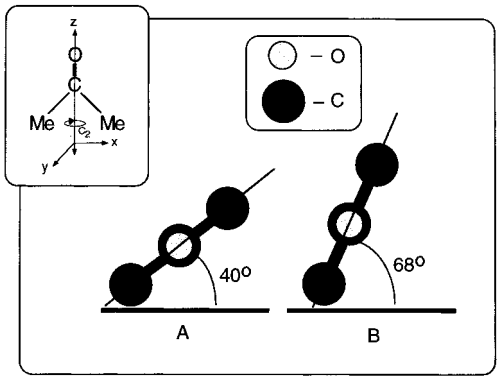

Figure 14. Proposed orientation model for acetone exposures less than (A) and higher than (B) 0.44 ML. The C═O bond is perpendicular to the plane of the paper. For clarity, the hydrogen atoms have been omitted from the figure. Inset: the C_2 axis of the acetone molecule (defined as *Z*) and the corresponding *X* and *Y* directions.

transient temperature rise at the surface under these conditions is 5.1 K, well below that needed to desorb acetone from Ag(111).

Prior work in our lab using continuous Hg arcs (250−400 nm) nm was confirmed:[23] postirradiation TPD contained no evidence for photon-driven chemistry at 248 nm. Similarly, with 193 nm irradiation, there was no TPD evidence for loss of parent or the formation of new products. Specifically, none of the following signals showed any structure: 43 amu (parent molecule), 2 amu (hydrogen), 15 amu (methyl), 16 amu (methane), 28 amu (carbon monoxide), 30 amu (ethane), 42 amu (ketene), and 86 amu (biacetyl). In only one situation was there a detectable signal—15 amu time of flight—but this signal appeared only for thick multilayers, and the signal-to-noise ratio precluded quantitative analysis. These results place an upper limit of order 10^{-21} cm^2 on cross sections associated with photons.

IV. Discussion

Thermal Properties. As is typical for Ag(111), the adsorption and desorption of CH_3COCH_3 occur with no dissociation. The activation energies estimated from the TPD data are 38 kJ mol^{-1} for α1 and 35 kJ mol^{-1} for α2 and α3, comparable to the molar heat of vaporization of acetone, 31 kJ mol^{-1}.[24] The α2 TPD peak saturates at approximately half the area of α1 (Figure 3), which is difficult to reconcile with a simple two-layer model that distinguishes α2 and α1. Were such a model realized, the α2 and α1 peak areas would be more nearly equal. Thus, α1 and α2 are assigned to the first layer, i.e., in contact with Ag, whereas α3 is attributed to multilayers. The distinction between α1 and α2 is the coverage-dependent structural rearrangement described below.

RAIRS. On the basis of IR symmetry rules, we expect only certain vibrational modes to be active, and of those, RAIRS on metals will detect only modes that have a component of the dynamic dipole moment perpendicular to the surface.[25] Assuming that the dynamic dipole moment of a weakly bound adsorbate does not change significantly with orientation, the observed absorbance is proportional to the $\cos^2(\theta)$, where θ is the angle between the direction of the dynamic dipole moment and the surface normal.[8−10,13] By comparing relative intensities of gas and adsorbed phases, we can identify preferred alignments of the adsorbates with respect to the surface normal.[13]

As applied to $(CH_3)_2CO$, we employ C_{2v} symmetry, with the 2-fold axis (defined as *z* in Figure 14) running along the CO bond.[26] The ν_a(MeCMe) and δ_s(Me) modes belong to the B_1 irreducible representation, while ν(CO), ν_s(MeCMe), and δ_a(Me) belong to A.

For a model with the two CH_3 groups and the carbonyl group all in contact with the surface, the *y*-axis is perpendicular to the surface; B_2 modes are allowed in this orientation. The only skeletal mode with this representation is the π(CO) mode, which has a vibrational frequency below 800 cm^{-1}, the cutoff for our spectra. Tilting slightly from this configuration, modes of other irreducible representations would become weakly active, as observed for the 0.56 ML case, i.e., weak absorption by the ν(CO), δ_s(Me), and ν_a(MeCMe) modes in Figure 5.

When the coverage is doubled to 1 ML, both the ν_a(MeCMe) and δ_s(Me) intensities increase 10-fold, far more than expected unless increased coverage is accompanied by a significant orientation change that brings the dynamic dipole moments of the B_1 irreducible representation closer to the surface normal. In other words, the *x*-axis of the molecule (insert of Figure 14) moves toward the surface normal. Unlike these intensity changes, the ν(CO) mode grows slowly and linearly, indicating that its dynamic dipole direction does not change appreciably in passing from 0.56 to 1.0 ML.

Figure 14 illustrates orientations consistent with these changes. With increasing coverage, the plane of the molecule moves closer to the surface normal, while the C═O bond always aligns nearly parallel to the surface plane. Using the gas-phase and adsorbed-phase relative intensities and a method based on the intensity of orthogonal vibrational modes,[6,18] we can extract, for the model in Figure 14, average alignment angles. Here, the ν(CO) mode is orthogonal to both the ν_a(MeCMe) and δ_s(Me). Using ν_a(MeCMe), the integrated absorbance ratio is

$$I_{\nu(\mathrm{CO})}/I_{\nu_a(\mathrm{MeCMe})} = [M_a \sin(\theta)^2 \nu_a G(x(\nu_a))]/[M_b{}^2 \cos(\theta)^2 \nu_b G(x(\nu_b))]$$

where the subscript "a" refers to the ν_a(MeCMe) mode, the subscript "b" refers to the ν(CO) mode, and θ is the angle between the C−C−C plane and the surface normal. $I_{\nu(\mathrm{CO})}$ and $I_{\nu_a(\mathrm{MeCMe})}$ refer to the integrated area of the absorbance peaks for these vibrations. Collecting all the constants gives

$$I_{\nu(\mathrm{CO})}/I_{\nu_a(\mathrm{MeCMe})} = C \tan(\theta)^2$$

If molecules were randomly oriented, as in the gas phase, the average θ would be 45°. For the gas phase, $I_{\nu(\mathrm{CO})}/I_{\nu_a(\mathrm{MeCMe})} = 2.23$. For an α1 exposure, this ratio is 3.19 and $\theta = 50°$, which corresponds to a C−C−C plane tilt of ∼40° away from the surface plane. For 1 ML coverage, $I_{\nu(\mathrm{CO})}/I_{\nu_a(\mathrm{MeCMe})} = 0.36$ and $\theta = 22°$ from the surface normal, and the average C−C−C plane tilts ∼68° away from the surface. Taking the uncertainty of the ν(CO) and ν_a(MeCMe) peak area measurements into account gives a range of 30°−66° for the α1 orientation and a range of 13°−29° for 1 ML.

As the coverage rises beyond 1 ML, both the A_1 and B_1 modes grow in proportion to the coverage increase, indicating that the average molecular orientation does not change further. The continued weakness of the carbonyl stretch intensity suggests that the acetone continues to layer in an organized pattern with all carbonyls nearly parallel to the surface. The low intensity of the ν(CO) mode was observed for coverages up to 15 ML, the highest coverage studied.

The splitting of the vibrational bands in Figure 5 is informative. At 0.53 ML, all three bands are adequately described by a single peak, but for higher coverages, especially multilayers, two peaks are required: the high-frequency component assigned to multilayer species and the low-frequency component to

adsorbates in the first layer, i.e, in contact with Ag(111). The splitting of ν(CO) mode is ~30 cm^{-1}, compared to ~ 5 cm^{-1} for ν_a(MeCMe) and δ_s(Me). This is consistent with a model involving considerable interaction between the π^* orbitals of the carbonyl and the valence band orbitals of Ag.

The ν(CO) spectrum requires further consideration, since it is split at monolayer coverage. This suggests, when $\alpha 1$ and $\alpha 2$ are saturated, that two adsorbate geometries are present, one of which removes the coupling of the carbonyl to Ag, while the other does not. Based on the other two modes, neither of these orientations lies in the multilayer.

We rule out the possibility that the low ν(CO) component is due to enol form CH_3COHCH_2. At room temperature in liquid acetone the enol fraction is less than 1%.[27] If a substantial portion of the acetone took on the enol form, we should see a C═C stretch near 1600 cm^{-1} and an O−H stretch between 3000 and 3200 cm^{-1}, neither of which we observe.

Several other molecules exhibit similar coverage-dependent orientation changes: methyl iodide on Mg(100),[8] alkyl halides on Pt(111),[9,10] methyl bromide on NaCl(001),[11] alkyl iodides on Ni(100),[28] and CF_3I on Ag(111).[13] Monte Carlo studies have predicted such changes for methyl halides on LiF(001).[12] Acetone is less symmetric but, like these, is polar. Consistent with earlier work, the rearrangement found here within the first layer can be related to the balance between adsorbate−substrate and interadsorbate interactions. As coverage increases, repulsive forces between the adsorbate molecules increase and, to keep the overall system energy at a minimum, drive an orientation change.[8,10,13]

The relative weakness of the ν(CO) mode in multilayers was unexpected, but it strongly suggests that alignment of the first monolayer forms a template that is preserved through multilayers. Evidently, there is sufficient anisotropy in the potential energy function describing the interaction of $(CH_3)_2CO$**(g)** with oriented $(CH_3)_2CO$**(a)** to maintain a nearly parallel alignment of C═O with the metal surface.

Electron Irradiation. As for numerous other adsorbates weakly held on Ag(111), $(CH_3)_2CO$ is vulnerable to electron irradiation with a sizable cross section (order of magnitude $10^{-17}-10^{-16}$ cm^2). This compares favorably to biacetyl[14] and methyl formate[20] but is an order of magnitude larger than for methanol.[21] All these adsorbates exhibit dissociation with retention of some fragments. Except for $HCOOCH_3$, there is also significant ejection during electron irradiation. For biacetyl, $CH_3COCOCH_3$, functionally comparable to $(CH_3)_2CO$, CH_3 and CO fragments dominate the ejection process, with much smaller contributions from ketene, CH_2CO, and ethane, C_2H_6. To account for the loss of C(1s) and O(1s) intensity in XPS, we propose that the same fragments are ejected here. For biacetyl, the postirradiation TPD includes peaks for methane at 235 K, ketene at 240 K, H_2 between 210 and 230 K, and biacetyl at 440 K.

All these features are evident in the work reported here and lead to the model depicted in Figure 15 for the electron irradiaton of oriented $(CH_3)_2CO$ on Ag(111) **(I)**. Electron irradiation leads to impact ionization and, as in conventional gas-phase mass spectrometry, subsequent fragmentation to form the following: (1) CO that is ejected **(II)** since it is not chemisorbed on Ag(111), (2) CH_3, some of which is ejected **(II)** and some retained **(III)**, and (3) CH_3CO, acetyl, which may be ejected, decompose into CO and CH_3, or be retained **(III)**. We also propose electron-induced rearrangement to the enol form **(IV)**. Thermal annealing **(III)** leads to some C−H bond breaking, desorbing ketene and providing active H that either hydrogenates CH_3 to CH_4 or recombines to desorb as H_2. Some recombination also occurs to re-form acetone. Finally, to account for the high-temperature acetone desorption, we propose that the enol form rearranges and promptly desorbs. For biacetyl, analogous fragments have been invoked to account for high-temperature parent desorption peaks.

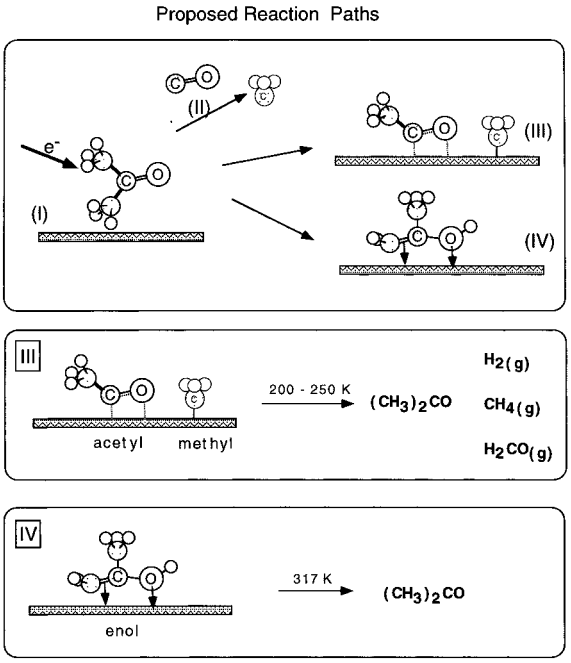

Figure 15. Schematic of proposed reaction routes for electron-initiated chemistry in the CH_3COCH_3−Ag(111) system.

Before irradiation, the orientation **(I)** deduced from RAIRS places one of the CH_3 groups away from the surface in a position that, intuitively, would favor desorption. Similarly, if the C−C bond adjacent to the surface ruptured, a CH_3CO group could be ejected and the CH_3 adjacent to the surface retained. Although not observed for any of the other oxygenated adsorbates, [14,20,21] parent desorption is also plausible. Note that the gas-phase fragmentation of acetone leads to significant amounts of CO^+, a multiple bond-breaking process that might be inhibited by quenching when near a surface. If CO is ejected, decomposition of excited CH_3CO in the vicinity of the surface might be responsible, a situation that could leave the CH_3 adsorbed. These issues could be addressed with angle- and velocity-resolved detection of ejected fragments using pulsed electron irradiation.

RAIRS after electron irradiation is quite informative. According to TPD (Figure 7), a fluence of 2.8×10^{15} e^- cm^2 reduces the initial TPD peak area by ~20%, whereas the RAIRS signals are reduced by 60% and 45% for the ν_a(MeCMe) and $\delta_s(CH_3)$ signals, respectively. The $\alpha 1$ state is preferentially depleted in TPD, while $\alpha 2$ does not change perceptibly with this fluence.

There is clearly more going on than multilayer removal. The TPD of parent changes dramatically, and new products appear in TPD. Were the effect due simply to removal of parent, then according to Figure 6, the intensity of the $\delta_s(CH_3)$ signal should drop more than the ν_a(MeCMe) signal. Just the opposite occurs. Further, the formation of products, an enol form of acetone, $CH_3CO_{(a)}H(CH_2)$, and acetyl, $CH_3C_{(a)}O_{(a)}$ (see Figure 15, species **III** and **IV**), cannot account for these changes. While each of these has a CH_3 group that would show a deformation mode, $\delta_s(CH_3)$, their frequencies would differ (not observed in Figure 6), and acetyl has no mode analogous to ν_a(MeCMe).

From this analysis, and that associated with the intensification of the carbonyl bands with irradiation, we propose that at low

fluences there is a large cross section for reorienting adsorbed CH_3COCH_3 such that the carbonyl group shifts direction, becoming more closely aligned with the surface normal. Simultaneously, the transition dipole moments associated with the $\delta_s(CH_3)$ and ν_a(MeCMe) modes also change their orientations with respect to the surface normal (and each other), such that ν_a(MeCMe) decays more strongly.

Photochemistry. The optical absorption of gas-phase acetone is characterized by a weak n $\rightarrow \pi^*$ transition in the 240−320 nm region (peak at 280 nm) and a series of much stronger structured Rydberg transitions setting in at ∼195 nm (n $\rightarrow$ 3s) and extending to lower wavelengths.[29] In neat liquid acetone, these intense structured transitions are not present and are replaced by much a much weaker, broader, and unstructured continuum extending from 195 nm down to 175 nm with a maximum around 185 nm. This continuum has been discussed in terms of a valence excitation (n $\rightarrow \sigma^*$). At 193 nm, the molar extinction coefficient in the neat liquid is approximately $\epsilon = 1000\ M^{-1}\ cm^{-1}$, while at 248 nm it it much weaker, $4\ M^{-1}\ cm^{-1}$.

Since, at monolayer and submonolayer coverages, no desorption products were observed in TPD or TOF and since thick multilayers (>5 ML) were required to observe even weak CH_3 fragment desorption, it appears that both substrate−adsorbate and adsorbate−adsorbate quenching compete with reactions to form new products. Arguably, the excited-state lifetime of acetone is too long (>100 fs) for dissociation along the repulsive curve to play a significant role; dissociation from the excited singlet and triplet state manifolds S1 and T1 is reported to require several rotational periods.[30] During this time interval, energy-transfer processes operate to quench the original excitation, thereby inhibiting product formation.

Compared to electron impact ionization, these photon excitations lead to quite different nascent excited states from which the chemistry evolves; ions with considerable internal energy are formed with electron excitation, while for photon excitation, neutral excited states form that, in the case of acetone, are not strongly dissociative.

V. Conclusions

The results can be summarized as follows:

The adsorption and desorption of CH_3COCH_3 on Ag(111) at 95 K occur with no dissociation.

Between 120 and 150 K, there are features attributable to monolayer and multilayer desorption peaks separated by no more than 12 K.

CH_3COCH_3 and CD_3COCD_3 are intermixed in TPD after sequential dosing at 90 K.

Both TPD and RAIRS exhibit features indicating structural changes as the first layer of adsorbate accumulates. From RAIRS, a model emerges in which the carbonyl axis always lies nearly parallel to the Ag surface, while the molecule's symmetry plane moves toward the surface normal as the coverage increases.

A 100 eV electron irradiation leads to dissociation accompanied by both ejection and retention of fragments.

TPD products observed after electron irradiation include $H_2(D_2)$, CH_4, CH_2CO, and CH_3COCH_3, the last formed by recombination/rearrangement of electron-induced species.

From RAIRS after irradiation, we conclude that electron irradiation also leads to reorientation of some of the residual CH_3COCH_3.

Up to 5 ML, there is no evidence for photochemistry upon irradiation with pulses of 248 or 193 nm. For 193 nm irradiation, there was a weak CH_3 ejection when the coverage exceeded 5 ML.

Acknowledgment. This work was supported in part by the National Science Foundation (CHE9319640) and by the Robert A. Welch Foundation.

References and Notes

(1) Avery, N. R. *Surf. Sci.* **1983**, *125*, 771. Vannice, M. A.; Erley, W.; Ibach, H. *Surf. Sci*. **1991,** *254*, 1.
(2) Sloan, D. W. Ph.D. Dissertation, University of Texas, 1996.
(3) Ayre, C. R.; Madix, R. J. *J. Am. Chem. Soc*. **1995,** *117*, 2301.
(4) Sexton, B. A.; Hughes, A. E. *Surf. Sci.* **1984,** *140*, 227.
(5) Avery, N. R.; Anton, A. B.; Toby, B. H.; Weinberg, W. H. *J. Electron Spectrosc. Relat. Phenom.* **1983**, *29*, 233
(6) Richardson, H. H. *J. Phys. Chem.* **1992,** *96*, 5898.
(7) Armstrong, J. L.; Langell, M.; White, J. M. *J. Vac. Sci. Technol*., in press.
(8) Fairbrother, D. H.; Briggman, K. A.; Stair, P. C.; Weitz, E. *J. Phys. Chem.* **1994,** *98*, 13042.
(9) French, C.; Harrison, I. *Surf. Sci.* **1995,** *342*, 85.
(10) Zaera, F.; Hofmann, H.; Griffiths, P. R. *J. Electron Spectrosc. Relat. Phenom.* **1990,** *54/55*, 705.
(11) Robinson, G. N.; Camilone III, N.; Rowntree, P. A.; Liu, G.; Wang, J.; Scoles, G. *J. Chem. Phys.* **1992,** *96*, 9212.
(12) Huang, Z.-H.; Guo, H. *J. Chem. Phys.* **1993,** *9*8, 7412.
(13) Szabo, A.; Converse, S. E.; Whaley, S. R.; White, J. M. *Surf. Sci.* **1996,** *364*, 345.
(14) Pylant, E. D.; Hubbard, M. J.; White, J. M. *J. Phys. Chem*. **1996**, *100*, 15890.
(15) Xu, J.; Jansch, H. J.; Yates, J. T. *J. Vac. Sci. Technol. A* **1993,** *11*, 726.
(16) McLafferty, F. W.; Stauffer, D. B. *The Wiley/NBS Registry of Mass Spectral Data;* Wiley: New York, 1989; Vol. 1.
(17) Sun, Z. J.; Schwaner, A. L.; White, J. M. *J. Chem. Phys.* **1995**, *103*, 4279. Junker, K. H.; Sun, Z.-J.; Scoggins, T. B.; White, J. M. *J. Chem. Phys*. **1996,** *104*, 3788.
(18) Dellepiane, G.; Overend, J. *Spectrochim. Acta* **1966,** *22*, 593.
(19) Curve a for ν(CO) may involve a small contribution at lower frequency, ca. 1682 cm^{-1}.
(20) Schwaner, A. L.; Fieberg, J. L.; White, J. M. *J. Phys. Chem*., submitted.
(21) Schwaner, A. L.; White, J. M. *Surf. Sci*., in preparation.
(22) The subscript "a" denotes atoms bound to Ag.
(23) Pressley, L. A.; Coon, S. A.; White, J. M., unpublished. Zhou, X.-L.; Zhu, X.-Y.; White, J. M. *Surf. Sci. Rep.* **1991**, *13*, 73. See, in particular, Table 1, p 146.
(24) Weast, R. C., editor-in-chief. *CRC Handbook of Chemistry and Physics*, 70th ed.; CRC Press: Boca Raton, FL, 1984.
(25) Woodruff, D. P.; Delchar, T. A. *Modern Techniques of Surface Science*, 2nd ed.; Cambridge University Press: Cambridge, 1994.
(26) Cotton, A. F. *Chemical Applications Of Group Theory*, 3rd ed.; John Wiley and Sons: New York, 1990.
(27) Solomons, T. W. G. *Organic Chemistry;* Wiley: New York, 1984.
(28) Tjandra, S.; Zaera, F. *J. Am. Chem. Soc.* **1995,** *117*, 9749.
(29) Robin, M. E. *Higher Excited States of Polyatomic Molecules;* Academic Press: New York, 1974.
(30) Kim, S. Y.; Pedersen, S.; Zewail, A. H. *J. Chem. Phys.* **1995,** *103*, 477. North, S. W.; Blank, D. A.; Gezelter, J. D.; Longfellow, C. A.; Lee, Y. T. *J. Chem. Phys.* **1995,** *102*, 4447.